AIAA 94-0428

# Soot Nucleation and Growth in Weakly-Buoyant Laminar Jet Diffusion Flames

Ü. Ö. Köylü, P.B. Sunderland, S. Mortazavi and G. M. Faeth
Department of Aerospace Engineering
The University of Michigan
Ann Arbor, Michigan

**32nd Aerospace Sciences Meeting & Exhibit**
January 10-13, 1994 / Reno, NV

# SOOT NUCLEATION AND GROWTH IN WEAKLY-BUOYANT LAMINAR JET DIFFUSION FLAMES

Ü.Ö. Köylü,* P.B. Sunderland,†
S. Mortazavi,† and G.M. Faeth**
Department of Aerospace Engineering
The University of Michigan
Ann Arbor, Michigan 48109-2118

## Abstract

An investigation of the structure and soot properties of weakly-buoyant laminar jet diffusion flames is described. A method for predicting the structure of soot-containing flames was developed, based on the conserved-scalar formalism in conjunction with the laminar-flamelet concept. The methodology was evaluated using measurements of flame shapes, and the distributions of mixture fractions, velocities and concentrations of major gas species, finding good agreement between predictions and measurements. The general properties of soot formation and oxidation in the weakly-buoyant flames was studied based on measurements of soot concentrations and structure as well as measurements of the local reactive environment. The results indicate that soot formation is associated with the presence of acetylene, that soot oxidation begins at fuel-rich conditions, and that soot nucleation and growth processes generally differ in buoyant and nonbuoyant flames due to different soot paths and residence time distributions in mixture fraction space.

## Nomenclature

| | | |
|---|---|---|
| $d$ | = | burner exit diameter |
| $d_p$ | = | primary soot particle diameter |
| $f$ | = | mixture fraction |
| $f_s$ | = | soot volume fraction |
| Fr | = | Froude number, $u_o^2/(gd)$ |
| $g$ | = | acceleration of gravity |
| $n_p$ | = | number of primary particles per unit volume |
| $p$ | = | pressure |
| $r$ | = | radial distance |
| Re | = | burner exit Reynolds number, $u_o d/\nu_o$ |
| $T$ | = | temperature |
| $u$ | = | streamwise velocity |
| $\boldsymbol{u}$ | = | velocity vector |
| $v$ | = | radial velocity |
| $X_f$ | = | mole fraction of fuel |
| $z$ | = | streamwise distance |
| $\mu$ | = | molecular viscosity |
| $\nu$ | = | kinematic viscosity |
| $\rho$ | = | density |
| $\sigma$ | = | Prandtl/Schmidt number |
| $\phi$ | = | fuel-equivalence ratio |

Subscripts

| | | |
|---|---|---|
| o | = | burner exit condition |

Superscripts

| | | |
|---|---|---|
| $(\,)^T$ | = | transpose of a tensor |

## Introduction

The scalar structure and soot properties of round laminar jet diffusion flames were studied in order to gain a better understanding of soot processes within nonpremixed flames. Effects of soot in nonpremixed flames are important because they influence the performance of propulsion systems, the hazards of unwanted fires, and the pollutant emissions from combustion processes. Although the properties of soot within turbulent flames are of the greatest practical interest, the present investigation was limited to laminar flames where detailed measurements are more tractable. Attention was confined to weakly-buoyant flames at low pressures in normal gravity. This was done in order to investigate the differences between soot properties in nearly nonbuoyant diffusion flames and the more widely studied buoyant diffusion flames. The measurements also were used to evaluate predictions of flame structure seeking a tractable approach to predict the structure of soot-containing diffusion flames, in view of current limited understanding of processes of fuel decomposition and soot chemistry.

A number of investigators have considered the structure of nonbuoyant laminar diffusion flames, using drop towers to provide a μg environment.[1-8] Quantitative measurements have been limited to flame lengths, with good agreement found between predictions based on the conserved-scalar formalism and measurements. Unfortunately, flame length is not a very sensitive indicator of model performance.[9,10] Additionally, the limited instrumentation and time capabilities of drop towers have prevented detailed studies of soot properties within nonbuoyant laminar diffusion flames.

In contrast, numerous studies of the structure and soot properties of buoyant laminar diffusion flames have been reported, see Glassman[11] for a recent review of work in the field. The coflowing laminar jet diffusion flame, that typically is used for measurements of laminar smoke point properties, has been a popular configuration for these studies. Among others, Santoro and Dobbins and coworkers have extensively studied this configuration at atmospheric pressure.[12-18] However, buoyancy causes soot to be confined to a narrow soot layer that is difficult to resolve experimentally, while the path that soot follows as it grows and oxidizes is completely different in buoyant and nonbuoyant flames, e.g., soot nucleation occurs near the flame sheet for buoyant flames but in the cooler core of the flow for nonbuoyant flames.[9,10] This raises questions about the relevance of findings for buoyant laminar flames to nonbuoyant flames which generally are of greatest practical interest.

Finally, detailed simulations of chemical kinetics have been successful for predicting the structure of methane/air flames where soot concentrations are relatively low.[19,20] However, corresponding methods for soot-containing flames will require substantial advances in the understanding of fuel decomposition and soot chemistry, while the computational tractability of such methods for practical flames is questionable. An attractive alternative involves the use of the conserved-scalar formalism, in conjunction with state relationships for scalar properties as a function of mixture fraction (called the laminar flamelet

* Research Fellow
† Graduate Student Research Assistant
** Professor, Fellow AIAA

approach), as proposed by Bilger.[21] In particular, measurements in soot-containing laminar diffusion flames show that state relationships for major gas species are relatively universal for combustion of a particular fuel type in air.[21-23] Furthermore, generalized state relationships have been found for a wide variety of hydrocarbon/air flames.[24] Thus, there appears to be potential for predicting the structure of laminar diffusion flames while avoiding both the uncertainties and complexities of detailed models of the chemistry of soot-containing environments, using the laminar flamelet approach. However, the accuracy and limitations of predictions based on the laminar flamelet approach have not been evaluated.

In view of this status, work has been initiated in this laboratory to study the structure and soot properties of weakly-buoyant and nonbuoyant laminar jet diffusion flames.[25-28] Initial studies involved evaluation of flame structure predictions based on the laminar flamelet concept using measurements of flame shapes and plume temperature distributions.[25,26] The resulting comparison between predictions and measurements was encouraging but flame shape predictions are not very definitive, as noted earlier. Initial measurements of soot properties within weakly-buoyant diffusion flames,[25,26] as well as measurements of the laminar smoke point properties of nonbuoyant diffusion flames,[27] highlighted significant differences between soot processes in buoyant and nonbuoyant laminar diffusion flames. Finally, these measurements have been exploited to seek a better understanding of soot formation in diffusion flames.[28]

The objectives of the present investigation were to extend the studies of Refs. 25-28 to consider: (1) a more complete evaluation of structure predictions using the laminar flamelet concept, and (2) observations of both soot properties and local flow properties within weakly-buoyant laminar jet diffusion flames, in order to gain a better understanding of soot processes in nonbuoyant diffusion flame environments. Present measurements include flame shapes using photography, soot volume fractions using laser extinction, temperatures using both thermocouples and multiline emission, soot structure using thermophoretic sampling and analysis by transmission election microscopy, concentrations of major gas species using sampling and analysis by gas chromatography, and velocities using laser velocimetry. Measurements were limited to weakly-buoyant laminar round jet diffusion flames fueled with either ethylene or acetylene and burning in air.

The paper begins with descriptions of experimental and theoretical methods. Results are then considered, treating flame structure and soot processes in turn.

## Experimental Methods

Test Apparatus. The present measurements of both flame structure and soot properties involved weakly-buoyant flames at ng. These experiments exploit the fact that buoyancy scales like $p^2g$ in laminar flames.[9,10] Thus, flames at pressures on the order of 0.1 atm have effective gravitational levels on the order of 0.01g, in comparison to flames at atmospheric pressure, and are weakly-buoyant if they are not too large. Thus, present measurements involved test flames from 3.3 mm diameter burners that had luminous regions that generally extended less than 50 mm from the burner exit. The ambient pressure range of the tests was 0.0625-0.250 atm, which provided a reasonable compromise between reduced soot concentrations at low pressures and increased effects of buoyancy at high pressures.

A sketch of the test apparatus appears in Fig. 1. The test configuration involved a round fuel jet injected vertically upward, surrounded by a slow concentric flow of air. The flames burned along the axis of a vertical cylindrical enclosure having a diameter and length of 300 mm. The top and bottom of the enclosure were porous metal plates which separated the enclosure from plenum chambers for air inflow and exhaust outflow, and provided a uniform distribution of air flow over the enclosure crossection. Air inflow was measured with a rotameter before passing through a pressure regulator to the air inlet plenum. The rotameter was calibrated using a wet test meter. The exhaust flow was removed using a vacuum pump.

The fuel flow port was aligned with the axis of the test enclosure with its exit 50 mm above the lower porous plate. The inside diameter of the fuel port was 3.3 mm, with the outside surface chamfered at an angle of 15° at the exit in order to minimize disturbances of the entrained air flow into the flames. The fuel flow passage had a flow straightener at the inlet followed by a constant area passage having a length-to-diameter ratio of 30:1 to yield fully-developed laminar pipe flow at the burner exit. The fuel flow was measured using a rotameter before passing through a pressure regulator to the fuel inlet plenum. The flames were ignited with a hot wire coil that could be placed near the burner exit and then rotated to a position near the chamber wall once the flames were ignited.

The flames were observed using four 110 mm diameter fused quartz windows located at 90° intervals around the side walls of the chamber. The axis of these windows was approximately 25 mm above the exit of the fuel port, which roughly centered the flames on the windows. The entire test chamber could be traversed in the vertical and horizontal directions in order to accommodate rigidly mounted optical instrumentation. Horizontal traversing was carried out using a stepping motor driven linear positioner having a positioning accuracy of 5 μm. Vertical traversing was carried out using a heavy duty laboratory jack having a manual positioning accuracy of 0.5 mm.

Instrumentation. Instrumentation included photography for measurements of flame shape, laser extinction for measurements of soot volume fractions, thermocouples and multiline emission for measurements of temperatures, thermophoretic sampling and analysis by transmission electron microscopy for measurements of sot structure, sampling and analysis by gas chromatography for measurements of the concentrations of major gas species, and laser velocimetry for measurements of velocities. The still photographs were taken in a darkened room using a 35 mm single lens reflex camera. The camera was directed through one of the side windows and had a field of view of 80 mm and a depth of field of 40 mm, which was sufficient to cover the luminous region of the flames. Color film was used so that yellow soot luminosity could be distinguished from the blue luminosity associated with the position of the flame sheet. The films were processed yield 100 × 125 mm color images which were used directly for measurements of flame shapes. The outlines of the blue and yellow regions could be measured with an accuracy of 0.5 mm.

The measurements of soot volume fractions involved deconvolution of laser extinction measurements at 632.8 nm for roughly 80 chord-like paths though the flames, following Santoro et al.,[12] similar to earlier work in this laboratory.[22,23] The soot volume fractions were computed assuming that soot aggregates satisfied the small particle (Rayleigh) scattering limit, while using the refractive indices of Dalzell and Sarofim,[29] which appear to best represent the properties of soot in diffusion flames.[30] Experimental uncertainties of soot volume fraction measurements (95% confidence) are estimated to be less than 15% for soot volume fractions greater than 0.1 ppm, increasing inversely proportional to soot volume fraction at lower values, while excluding effects of uncertainties of the refractive indices of soot.

Gas temperatures were measured using bare wire thermocouples, constructed from 125 μm diameter

platinum/platinum-10% rhodium wire, in regions where soot was absent. The junctions had a diameter of 270 μm and were roughly spherical in shape, with the thermocouple leads extending roughly 20 wire diameters in the streamwise direction in order to minimize conductions errors. Effects of convection on heat transfer to the junctions were small for present conditions so that radiative heat loss corrections were found assuming a Nusselt number equal to 2, with the junction surface emissivity taken from Bradley and Entwhistle.[31] Experimental uncertainties (95% confidence) for thermocouple measurements were less than 50K, dominated by the uncertainties of thermocouple junction emissivities.

Thermophoretic deposition of soot prevented the use of thermocouples for temperature measurements where soot was present. Instead, temperatures within soot-containing regions were found using multiline emission measurements, similar to past work.[32-34] This method involved deconvoluting emission measurements at 600, 700, 750 and 830 nm for roughly 80 cordlike paths through the flames. These results were analyzed to find temperature distributions within the flames based on the following assumptions: soot optical properties approximated using the small particle (Rayleigh) scattering limit; the flames were assumed to be optically thin, which was justified based on measured transmittivities greater than 85-90%; and variations of refractive indices were neglected over the wavelength range of interest, based on the measurements of Dalzell and Sarofim.[29] Temperatures were estimated by averaging results for three line pairs — 600/750 nm, 700/830 nm and 600/830 nm. These results proved to be consistent, e.g., temperature differences between the average and any of the line pairs were less than 30K. Experimental uncertainties (95% confidence ) of these measurements are estimated to be less than 50K.

Soot structure was measured using thermophoretic sampling and analysis using transmission electron microscopy (TEM) similar to Megaridis and Dobbins[15,16] but following specific methods due to Köylü and Faeth.[35] The sampling surfaces were the 3 mm diameter copper grids used to hold TEM specimens (200 mesh copper grids supported by a 20 nm thick elemental carbon film). The grids were mounted on a retractable probe using Data Coat glue, with the grids aligned parallel to the streamwise direction at the flame axis during sampling. The probe was stored in a cylinder with roughly a 50 mm stroke to reach the flame axis. A double acting pneumatic cylinder rapidly drove the probe out of the storage cylinder to the sampling position and returned it to the cylinder when sampling was complete. Sampling times were controlled so that no more than 10% of the TEM grid surface was covered with soot aggregates to prevent overlapping aggregates; this required 30-36 ms sampling times, compared to 2-3 ms traveling times of the grid through the flames to the axis. The details of TEM analysis were identical to past work.[35] Effects of soot aggregate size cause negligible sampling bias for present test conditions,[35,36] yielding experimental uncertainties (95% confidence) dominated by finite sampling limitations, as follows: primary soot particle diameters less than 5% and mean numbers of primary particles per soot aggregate less than 20%. The mean number of primary particles per unit volume was computed from the measured values of $f_s$ and $d_p$, as follows:

$$n_p = 6f_s / (\pi d_p^3) \qquad (1)$$

Thus, based on the uncertainties of $f_s$ and $d_p$ the experimental uncertainties (95% confidence) of $n_p$ are less then 21% for values of $f_s$ greater than 0.1 ppm.

Gas compositions were measured along the axis of the flames by sampling and analysis using gas chromatography, similar to earlier work.[22,23] A stainless steel radiatively cooled probe was used, with a relatively large (3.3 mm) sampling port diameter in order to minimize problems of clogging by deposited soot. The probe was traversed along the axis of the flames using a stepping motor driven linear positioner. Thus, soot deposited on the probe could be burned off periodically by traversing the probe to a soot oxidation region. Concentrations of CO, $CO_2$, $O_2$, $N_2$, $H_2$, $CH_4$, $C_2H_6$, $C_2H_4$ and $C_2H_2$ were measured directly, while concentrations of $H_2O$ then found by assuming that the C/H ratio of the fuel was preserved. Experimental uncertainties (95% confidence) of these fractions greater than 0.5%, largely dominated by uncertainities in measuring chromatogram peak areas.

Streamwise velocities along the axis of the flames were measured using a dual-beam forward scatter laser velocimeter (LV) based on the 514.5 nm line of an argon-ion laser operating with 1200 mW of optical power. The optical arrangement provided a measuring volume having a diameter and length of 240 and 720 μm. the laser power was strong enough so that soot particles provided adequate seeding when they were present; this was supplemented by aluminum oxide particles having a nominal diameter of 0.5 μm for the region near the burner exit. The LV scattering signals were processed using a burst counter to provide experimental uncertainties (95% confidence) less than 5% over the range of the measurements, mainly dominated by finite sampling time and calibration uncertainties.

Acetylene Purity. A problem with the use of acetylene as a test fuel involves contamination by acetone that is placed within acetylene gas cylinders due to safety concerns.[37] The effect of acetone contamination was evaluated by passing the fuel gas through the purifying train described by Hamins et al.,[37] which reduced acetone mole fractions to less than 0.1%. It was found that this level of removal of acetone had a negligible effect of soot properties within the present test flames, which always involved acetone mole fractions less than 2%.

## Theoretical Methods

The predictions of flame structure were based on the following major assumptions: steady laminar axisymmetric flow; constant radiative heat loss fraction of the chemical energy release for all parts of the flame; the laminar flamelet approximation for all scalar properties, which requires the previous radiation approximation and implies equal binary diffusivities of all species, negligible thermal diffusion and unity Lewis number; small flame standoff distance at points of flame attachment; ambient environment has constant properties; ideal gas mixtures with negligible soot volumes and a constant Prandtl/Schmidt number; and multicomponent mixing laws to find the mixture viscosity. Steady laminar axisymmetric flow is a condition of the experiment while the other approximations all are aspects of the laminar flamelet approach which is being tested.[21-24]

Present measurements involved ethylene and acetylene/air flames at pressures of 0.0625-0.250 atm. Thus, earlier measurements of the state relationships for these fuels burning in air atmospheric pressure, Refs. 22-24, were supplemented by measurements at lower pressures during the present investigation. Typical results for acetylene/air flames are illustrated in Fig. 2 where the mole fractions, of major gas species ($C_2H_2$, $N_2$, $O_2$, $CO_2$, CO, $H_2O$ and $H_2$) are plotted as a function of fuel-equivalence ratio (which is a single-valued function of the mixture fraction). The measurements extend over the pressure range 0.125-1.000 atm, drawing results at 1 atm from Gore and Faeth,[23] and involve a range of burner Reynolds numbers, buoyancy conditions and positions in the flames. Predictions based on the assumption of thermodynamic equilibrium, using the Gordon and McBride[38] algorithm, also are shown on the plots. In general, the plots yield universal correlations between the concentrations of major gas species and mixture fractions, expected for the laminar flamelet concept,[21-24] over the test range. The only significant exceptions are the concentrations of $CO_2$ and CO at fuel-rich conditions where the results of Gore and Faeth[23] are somewhat high at 1 atm for $CO_2$, and the present results are somewhat high for CO at 0.125

atm. On the other hand, the generalized state relationships for hydrocarbon/air flames,[24] are in good agreement with the results plotted in Fig. 2, aside from the exceptions just noted. Thus, use of the same state relationships for a particular fuel/air diffusion flame appears to be acceptable over the range of pressures considered during the present investigation. Given the state relationships for major gas species, and the radiative heat loss fractions, the state relationships for temperature were computed as described in Ref. 24.

Present test conditions involved modest maximum burner exit Reynolds numbers, Re ca. 100; therefore, the full elliptic governing equations were solved rather than adopting the boundary layer approximations. Based on these assumptions the following governing equations for conservation of mass, momentum and mixture fraction must be solved:

$$\nabla \cdot (\rho \mathbf{u}) = 0 \tag{2}$$

$$\nabla \cdot (\rho \mathbf{u}\mathbf{u}) = \rho \mathbf{g} - \nabla p - \nabla \cdot (\mu \nabla \mathbf{u} + \nabla \mathbf{u}^T)) \tag{3}$$

$$\nabla \cdot (\rho \mathbf{u} f) = \nabla \cdot (\mu \nabla f) / \sigma \tag{4}$$

The boundary conditions across the burner exit involved f=1 by definition and fully-developed laminar pipe flow. The remaining boundary conditions allowed for the air coflow and the chamber geometry. The equations were solved following Patankar[39] with a variable grid spacing and a 60 (radial) × 88 (streamwise) mesh. Computations for various grids indicated numerical accuracy within 1-2%.

## Results and Discussion

### Flame Structure

Flame shapes were used for the initial evaluation of the predictions. The predicted locations of the flames were taken to be the locus of stoichiometric conditions, $\phi = 1$; the measured flame locations were taken to be the locus of the blue-emitting flame sheet. Typical flame shape predictions and measurements for weakly-buoyant laminar jet diffusion flames are illustrated in Figs. 3 and 4. These results are for ethylene and acetylene/air flames at ambient pressures of 0.0625-0.250 atm and a range of burner exit Reynolds numbers. The experimental results are terminated when yellow luminosity from soot prevented observation of the blue flame boundary. Effects of buoyancy, ambient pressure and coflow are relatively weak; therefore, the main effect of reduced ambient pressures is to increase both the maximum width of the flames and the extent of the region where the blue flame sheet can be observed (the last because soot concentrations are lower at lower pressures). The comparison between predictions and measurements is good, including proper treatment of effects of Re, fuel type and pressure on flame shapes, and the tendency of the flames to attach somewhat below the exit of the burner due to streamwise diffusion. As noted earlier, the comparison between predicted and measured temperature distributions in the fuel-lean region of the flames also was quite good, well within experimental uncertainties.

The final evaluation of the laminar-flamelet approach involved velocity, mixture fraction and major gas species concentrations along the axis of weakly-buoyant laminar jet diffusion flames. Typical results are illustrated in Fig. 5 for an acetylene/air flame at 0.25 atm and Re = 80. In particular, the state relationships properly account for the low levels of oxygen observed before the fuel is completely consumed, followed by more rapid growth of oxygen concentrations beyond the flame tip. As noted in connection with Fig. 4, the location of the flame tip is predicted accurately because the predicted distribution of mixture fractions is in good agreement with the measurements. The velocity profiles highlight some of the problems of observing nearly nonbuoyant flames of reasonable size at ng. Near the jet exit, velocities decay rapidly, which is consistent with nonbuoyant laminar jet diffusion flame behavior. However, farther from the jet exit, velocities slowly begin to increase as effects of buoyancy become more significant. The predictions represent this behavior reasonably well, however, the measurements clearly are not representative of truly nonbuoyant flame behavior.

Taken together, the results discussed in connection with Figs. 2-5, along with earlier findings,[25] implies reasonably successful use of the laminar flamelet concept for predictions of the structure of soot-containing flames. This provides a way of circumventing current uncertainties about fuel decomposition and soot chemistry in soot-containing flames that would be required for more detailed simulations. While state relationships for specific fuels (ethylene and acetylene) burning in air were used during current work, the existence of generalized state relationships[24] suggests that the methodology can be extended to other hydrocarbons burning in air. Nevertheless, evaluation of this generalization still is required. Conversely, the existence of generalized state relationships raises interesting questions about the chemical kinetics of hydrocarbon fuel decomposition in diffusion flames that have yet to be explored.

### Soot Processes

Test conditions used to study soot processes in laminar diffusion flames are summarized in Table 1. The burner flows involved $C_2H_2/N_2$ mixtures with combustion in coflowing air at pressures of 0.125-0.250 atm. Visible flame lengths were maintained at roughly 50 mm (z/d = 15.2) in order to provide reasonable spatial resolution for the measurements. The corresponding characteristic residence times of the flames, defined as the time required for a fluid parcel to convect along the axis from the burner exit to the flame tip (where the mixture at the axis is stoichiometric) were in the range 16.9-22.6 ms. These conditions involved burner Reynolds and Froude numbers in the ranges 80-149 and 27-256, respectively. Measurements of radiative heat fluxes from the flames indicated radiative heat loss fractions in the range 29-34% of the lower heating value (LHV) of the burner flow.

Radial distributions of soot volume fractions for Flame 1 are illustrated in Fig. 6; results for the other flames were similar. The measurements involve various values of z/d in the range 1.9-15.2. An annular soot layer, similar to the soot layers observed in buoyant laminar jet diffusion flames,[12-18] begins to form near the burner exit, with soot building up later near the axis as the flame sheet is reached at the axis (corresponding to the flame tip) when z/d = 9.5 for Flame 1 (see Table 1). Soot oxidation extends to the axis in the vicinity of the flame tip and beyond, with soot concentrations becoming small at all radial distances far from the burner exit in this nonsooting flame. The breadth of the soot-containing region, and its uniformity far from the burner exit, provides improved spatial resolution for measurements of soot processes in weakly-buoyant flames, when compared to buoyant flames where the soot layers approach the axis more closely near the end of the luminous flame region.[12-18]

Motion along a soot path line involves a monotonic reduction of mixture fraction (or fuel-equivalence ratio) for the weakly-buoyant flame of Fig. 6, except for a small region near the base of the flame.[27] Then, the temperature increases as the flame sheet is approached at fuel-rich conditions, which eventually initiates soot nucleation and growth, and causes soot concentrations to reach a maximum near the flame sheet. Soot oxidation begins subsequently and continues within the fuel-lean region, causing soot concentrations to decrease and eventually become zero if the flame is nonsooting. TEM photographs of soot in these flames are presented elsewhere.[28] In general the soot in present flames was typical of past observations[15,16] and consisted of roughly spherical primary soot particles, having nearly constant diameters at a particular flame condition, collected into aggregates having widely varying numbers of primary particles per aggregate.

A more detailed picture of soot and flame properties within weakly-buoyant laminar jet diffusion flames can be obtained from the results plotted in Fig. 7. Here, measurements along the axis for all four test flames are plotted as a function of residence time, which is defined as the time required for the flow to convect from the burner exit to the position being considered. The following parameters are plotted in the figure (reading from the top): soot volume fraction, mean primary particle diameter, number of primary particles per unit volume, temperature, and fuel (acetylene) mole fraction.

An interesting feature of the results illustrated in Fig. 7 is that $d_p$ often is largest near the start of soot formation. This highlights an observation of Tesner,[40] who notes that surface growth persists at temperatures much lower than those required to initiate soot particle nucleation (inception). This property causes rapid growth of the limited number of soot particles present near the start of the soot formation region, producing rather large primary particles. Subsequently, accelerating nucleation rates create additional primary soot particles whose shorter growth period causes $d_p$ to decrease, even though overall soot concentration levels (represented by $f_s$) are increasing.

For the results plotted in Fig. 7, significant levels of soot formation (based on increasing values of soot volume fractions) only is observed when temperatures exceed 1250-1600 K. The end of soot formation, based on the maximum value of $f_s$ being reached (noting that gas densities are relatively uniform in the region where soot growth is observed), generally occurs when the concentration of acetylene becomes small, which is well before the flame sheet is reached, i.e., at a fuel-equivalence ratio of roughly 1.7. Notably, nucleation also ceases when the maximum value of $f_s$ is reached, which corresponds to conditions where acetylene disappears as just noted. Thus, the presence of acetylene appears to be a prerequisite for both soot nucleation and growth.

Comparing results for the four test flames in Fig. 7 yields general trends concerning effects of pressure and fuel concentration on soot properties. It should be recalled, however, that the four test flames are somewhat arbitrary and while they have similar flame lengths, they involve a variety of reaction environments and residence times (see Table 1). First of all, the effect of pressure on soot concentrations is seen to be substantial by comparing results for Flames 1, 2 and 3; in fact, maximum soot concentrations are proportional to $p^2$ for present test conditions. This strong effect of pressure is reasonable, however, because reduced pressures are expected to reduce both soot formation rates and available residence times for present test conditions.[27] Another effect of reduced pressure is to generally increase flame temperatures along the axis (see Fig. 7) and decrease radiative heat loss fractions (see Table 1). These effects are a direct consequence of reduced soot concentrations at low pressures, which reduces continuum radiative heat losses from the flames.

The effect of diluting the fuel with nitrogen at a fixed total pressure can be seen by comparing results for Flames 1 and 4 in Fig. 7. In this case, both the residence time (see Table 1) and the temperature distributions (see Fig. 7) of the two flames are nearly the same; therefore, the substantially reduced concentrations of soot in the diluted flame must be attributed to reduced concentrations of the reactant acetylene. It should be noted, however, that this explanation of the effect of diluting the fuel with nitrogen differs from that of Glassman and coworkers,[11] where effects of fuel dilution on laminar smoke point properties are attributed to modified flame temperatures. Nevertheless, the rather direct explanation that reduced reactant concentrations imply reduced soot concentrations is more appropriate for present conditions. This behavior occurs because fuel dilution has a relatively small effect on adiabatic flame temperatures and even this small effect is compensated by reduced radiative heat losses due to reduced soot concentrations.

Finally, effects of soot nucleation and growth for the four flames illustrated in Fig. 7, combine to yield relatively complex behavior for $d_p$ during the soot formation stage. In particular, $d_p$ tends to increase early in the soot formation period, however, accelerating rates of soot nucleation cause $d_p$ to generally decrease during the later stages of the soot formation, as discussed earlier. In contrast, the behavior $d_p$ is straightforward in the soot oxidation period, progressively decreasing with increasing residence time as anticipated.

These results suggest that the different locations for nucleation of most of the soot in nonbuoyant and buoyant diffusion flames plays a large role in other differences of soot processes for these flames. In particular, most soot nucleates near the cool core of nonbuoyant diffusion flames, which causes initial rapid growth of primary particle diameters. However, as temperatures increase along a soot path in a nonbuoyant flame, rates of nucleation increase causing primary soot particle diameters to reach a maximum early in the soot formation period. In contrast, most soot nucleates near the flame sheet in buoyant diffusion flames. Then, the soot path initially toward the cool core allows growth to proceed progressively, with reduced rates of nucleation, so that primary particle diameters and soot concentrations correspond more closely. Naturally, different distributions of flow velocities and mixture fractions along soot paths also contribute to different soot properties within nonbuoyant and buoyant flames.[29]

## Conclusions

The structure and soot properties of weakly-buoyant laminar jet diffusion flames were studied. The major conclusions of the investigation are as follows:

1. State relationships for major gas species appear to be a relatively robust property of laminar soot-containing diffusion flames. This provides a useful simplification for predicting the structure of these flames, based on the conserved-scalar formalism, that circumvents the need to consider processes fuel decomposition and soot chemistry that are not understood very well at the present time.

2. Hydrocarbons burning in air, with initial fuel and air stream temperatures near room temperature, yield generalized state relationships relatively independent of fuel type and pressure. Processes of stoichiometry explain this behavior for fuel lean conditions,[24] however, why this remarkable behavior occurs at fuel-rich conditions has not been explained and certainly merits additional attention.

3. Present observations of soot structure in nonbuoyant diffusion flames were generally similar to observations in buoyant diffusion flames, with soot consisting of nearly spherical primary particles collected into wispy aggregates. Primary particle diameters exhibited more complex behavior in nonbuoyant than buoyant diffusion flames, however, reaching a maximum before maximum soot concentrations were reached that suggests a stronger temperature dependence for nucleation than growth rates.

4. Soot formation (nucleation and growth) is associated with the presence of acetylene, given sufficiently high temperatures (1250-1600 K) for reasonable levels of soot nucleation to occur. Thus, since acetylene disappears at a fuel-equivalence ratio of roughly 1.7 in the present flames, soot formation stops and soot oxidation begins at fuel-rich conditions along a soot path.

Acknowledgments

This research was sponsored by NASA Grant No. NAG3-1245, under the technical management of D. L. Urban of the Lewis Research Center, and the Office of Naval Research Grant No. N00014-93-0321 under the technical management of G. G. Roy. The authors would like to acknowledge helpful discussions with M.B. Colket, III, R. A. Dobbins, H. B. Palmer, R.J. Santoro and K. Seshadri

References

[1]Cochran, T.H., and Masica, W.J., "An Investigation of Gravity Effects on Laminar Gas Jet Diffusion Flames," *Thirteenth Symposium (International) on Combustion*, The Combustion Institute, Pittsburgh, 1970, pp. 821-829.

[2]Haggard, J.B. Jr., and Cochran, T.H. "Stable Hydrocarbon Diffusion Flames in a Weightless Environment," Combust. Sci. Tech., Vol. 5, 1972, pp. 291-298

[3]Edelman, R.B., Fortune, O.F., Weilerstein, G., Cochran, T.H., and Haggard, J.B., Jr., "An Analytical and Experimental Investigation of Gravity Effects upon Laminar Gas Jet-Diffusion Flames," *Fourteenth Symposium (International) on Combustion*, The Combustion Institute, Pittsburgh, 1972, pp. 399-412.

[4]Klajn, M., and Oppenheim, A.K., "Influence of Exothermicity on the Shape of a Diffusion Flame," *Nineteenth Symposium (International) on Combustion*, The Combustion Institute, Pittsburgh, 1982, pp. 223-235.

[5]Edelman, R.B., and Bahadori, M.Y., "Effects of Buoyancy on Gas-Jet Diffusion Flames: Experiment and Theory," Acta Astronautica ,Vol. 13, 1986, 681-688.

[6]Bahadori, M.Y., Edelman, R.B., Stocker, D.P., and Olson, S.L., "Ignition and Behavior of Laminar Gas-Jet Diffusion Flames in Microgravity," AIAA J., Vol. 28, 1990, pp. 236-244.

[7]Bahadori, M. Y., Stocker, D. P., and Edelman, R. B., "Effects of Pressure on Microgravity Hydrocarbon Diffusion Flames," AIAA Paper No. 90-0651, 1990.

[8]Bahadori, M.Y., Edelman, R.B., Stocker, D.P., Sotos, R.G., and Vaughan, D.F., "Effects of Oxygen Concentration on Radiative Loss from Normal-Gravity and Microgravity Methane Diffusion Flames," AIAA Paper No. 92-0243, 1992.

[9]Faeth, G. M., "Homogeneous Premixed and Nonpremixed Flames in Microgravity: A Review," *Proceedings of the AIAA/IKI Microgravity Science Symposium*, AIAA, Washington, 1991, pp. 281-293.

[10]Law, C.K., and Faeth, G.M., "Opportunities and Challenges of Combustion in Microgravity," Prog. Energy Combust. Sci., submitted.

[11]Glassman, I., "Soot Formation in Combustion Processes," *Twenty-Second Symposium (International) on Combustion*, The Combustion Institute, Pittsburgh, 1988, pp. 295-311.

[12]Santoro, R.J., Semerjian, H.B., and Dobbins, R.A., "Soot Particle Measurements in Diffusion Flames," Combust. Flame, Vol. 51, 1983, pp. 203-218.

[13]Santoro, R.J., Yeh, T.T., Horvath, J.J., and Semerjian, H.G., "The Transport and Growth of Soot Particles in Laminar Diffusion Flames," Combust. Sci. Tech., Vol. 53, 1987, pp. 89-115.

[14]Dobbins, R.A., and Megaridis, C.M. "Morphology of Flame-Generated Soot as Determined by Thermophoretic Sampling," Langmuir, Vol. 3, 1987, pp. 254-259.

[15]Megaridis, C.M., and Dobbins, R.A., "Comparison of Soot Growth and Oxidation in Smoking and Nonsmoking Ethylene Diffusion Flames," Combust. Sci. Tech., Vol. 66, 1989, pp. 1-16.

[16]Megaridis, C.M., and Dobbins, R.A., "Morphological Description of Flame-Generated Materials," Combust. Sci. Tech., Vol. 77, 1990, pp. 95-109.

[17]Dobbins, R.A., Santoro, R.J., and Semerjian, H.G., "Analysis of Light Scattering from Soot Using Optical Cross Sections for Aggregates," *Twenty-Third Symposium (International) on Combustion*, The Combustion Institute, Pittsburgh, 1990, pp. 1525-1532.

[18]Puri, R., Richardson, T.F., Santoro, R.J., and Dobbins, R.A., "Aerosol Dynamic Processes of Soot Aggregates in a Laminar Ethene Diffusion Flame," Combust. Flame, Vol. 92, 1993, pp. 320-333.

[19]Rogg, B., "On Numerical Analysis of Two-Dimensional, Axisymmetric, Laminar Jet Diffusion Flames," *Mathematical Modeling in Combustion and Related Topics* (C.-M. Brauner and C. Schmidt-Laine, eds.), Martinus Nijhoff Publishers, Amsterdam, 1988, pp. 551-560.

[20]Smooke, M.D., Mitchell, R.E., and Keyes, D.E., "Numerical Solution of Two-Dimensional Axisymmetric Laminar Diffusion Flames," Combust. Sci. Tech., Vol. 67, 1989, pp. 85-122.

[21]Bilger, R. W., "Reaction Rates in Diffusion Flames," Combust. Flame, Vol. 30, 1977, pp. 277-284.

[22]Gore, J.P., and Faeth, G.M., "Structure and Spectral Radiation Properties of Turbulent Ethylene/Air Diffusion Flames," *Twenty-First Symposium (International) on Combustion*, The Combustion Institute, Pittsburgh, 1986, pp. 1521-1531.

[23]Gore, J.P., and Faeth, G.M., "Structure and Radiation Properties of Luminous Turbulent Acetylene/Air Diffusion Flames," J. Heat Trans., Vol. 110, 1988, pp. 173-181.

[24]Sivathanu, Y.R., and Faeth, G.M., "Generalized State Relationships for Scalar Properties in Nonpremixed Hydrocarbon/Air Flames," Combust. Flame, Vol. 82, 1990, pp. 211-230.

[25]Mortazavi, S., Sunderland, P.B., Jurng, J., Köylü, Ü.Ö., and Faeth, G.M., "Structure of Soot-Containing Laminar Jet Diffusion Flames," AIAA Paper No. 93-0708, 1993.

[26]Faeth, G.M., Sunderland, P.B., Köylü, Ü.Ö., and Urban, D.L., "Laminar Jet Diffusion Flames in Microgravity: A Paradigm for Soot Processes in Turbulent Flames," Proceedings of International Symposium on Aerospace and Fluid Sciences, Sendai, Japan, 1993, pp. 185-198.

[27]Sunderland, P.B., Mortazavi, S., Faeth, G.M., and Urban, D.L., "Laminar Smoke Points of Nonbuoyant Jet Diffusion Flames," Combust. Flame, in press.

[28]Sunderland, P.B., Köylü, Ü.Ö., and Faeth, G.M., "Soot Formation in Weakly-Buoyant Acetylene-Fueled Laminar Jet Diffusion Flames Burning in Air," *Twenty-Fifth Symposium (International) on Combustion*, The Combustion Institute, Pittsburgh, submitted.

[29]Dalzell, W.H., and Sarofim, A.F., "Optical Constants of Soot and Their Application to Heat Flux Calculations," J. Heat Trans., Vol. 91, 1969, pp. 100-104.

[30]Köylü, Ü.Ö., and Faeth, G.M., "Optical Properties of Overfire Soot in Buoyant Turbulent Diffusion Flames at Long Residence Times," J. Heat Trans., in press.

[31]Bradley, D., and Entwistle, A.C., "Determination of the Emissivity, for Total Radiation, of Small Diameter Platinum-10% Rhodium Wires in the Temperature Range 600-1450°C," British J. Appl. Phys. Vol.. 12, 1961, pp. 708-711.

[32]Cashdollar, K.L., "Three-Wavelength Pyrometer for Measuring Flame Temperatures," Appl. Optics Vol. 18, 1979, pp. 2595-2597.

[33]Klingenberg, G., "Invasive Spectroscopic Technique for Measuring Temperature in Highly Pressurized Combustion Chambers," Optical Engineering Vol. 24, 1985, pp. 692-696.

[34]Sivathanu, Y.R., and Faeth, G.M., "Temperature/Soot Volume Fraction Correlations in the Fuel Rich Region of Buoyant Turbulent Diffusion Flames," Combust. Flame Vol. 81, 1990, pp. 150-165.

[35]Köylü, Ü.Ö., and Faeth, G.M., "Structure of Overfire Soot in Buoyant Turbulent Diffusion Flames at Long Residence Times," Combust. Flame, Vol. 89, 1992, pp. 140-156.

[36]Rosner, D.E., Mackowski, D.W., and Garcia-Ybarra, P., "Size- and Structure-Insensitivity of the Thermophoretic Transport of Aggregated Soot Particles," Combust. Sci. Tech., Vol. 80, 1991, pp. 87-101.

[37]Hamins, A., Gordon, A.S., Saito, K., and Seshadri, K., "Acetone Impurity in Acetylene from Tanks," Combust. Sci. Tech., Vol. 45, 1986, pp. 309-310.

[38]Gordon, S., and McBride, B. J., "Computer Program for Calculation of Complex Chemical Equilibrium Compositions, Rocket Performance, Incident and Reflected Shocks, and Chapman-Jouguet Detonations," NASA SP-273, 1971.

[39]Patankar, S.V., *Numerical Heat Transfer and Fluid Flow*, McGraw-Hill, New York, 1980.

[40]Tesner, P.A., "Formation of Dispersed Carbon by Thermal Decomposition of Hydrocarbons," *Seventh Symposium (International) on Combustion*, The Combustion Institute, Pittsburgh, 1958, pp. 546-553.

Table 1. Summary of soot property test flames[a]

| Test Flame | 1 | 2 | 3 | 4 |
|---|---|---|---|---|
| Pressure (atm) | 0.250 | 0.188 | 0.125 | 0.250 |
| Burner flow (% $C_2H_2$ by vol.) | 100 | 100 | 100 | 58 |
| $C_2H_2$ flow rate (cc/s) | 8.12 | 13.6 | 25.0 | 8.96 |
| $N_2$ flow rate (cc/s) | --- | --- | --- | 6.24 |
| Air flow rate (cc/s) | 395 | 755 | 1450 | 395 |
| Stoich. flame length (z/d) | 9.5 | 13.9 | 15.2 | 12.2 |
| Char. res. time (ms) | 19.7 | 22.6 | 16.9 | 19.4 |
| Re (-) | 80 | 100 | 122 | 149 |
| Fr (-) | 27 | 76 | 256 | 96 |
| Rad. heat loss (% LHV) | 34.2 | 32.3 | 29.4 | 31.7 |

[a]Laminar round jet diffusion flames with 3.3 mm inside diameter burner and a visible flame length of roughly z/d = 15.2.

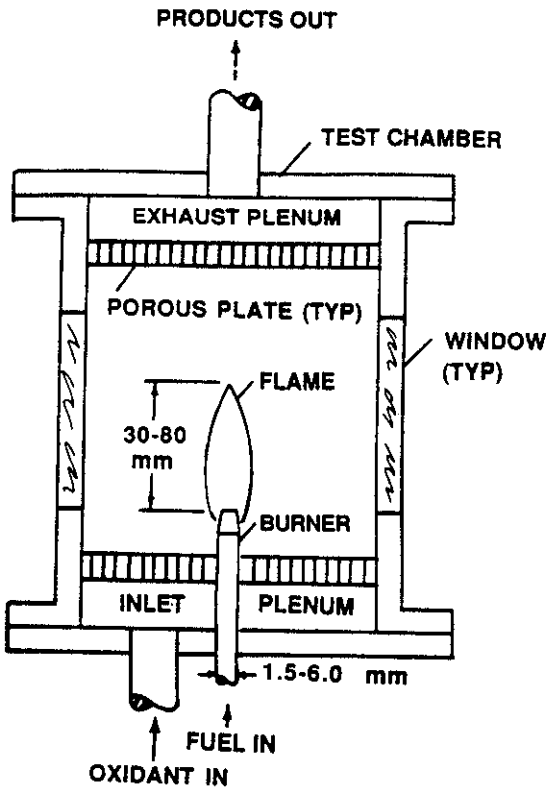


Fig. 1 Sketch of the experimental apparatus.

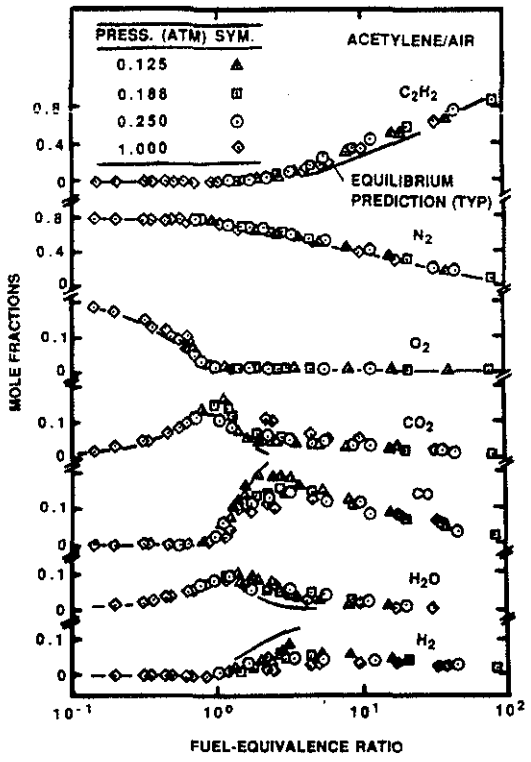


Fig. 2 State relationships for major gas species in acetylene/air diffusion flames.

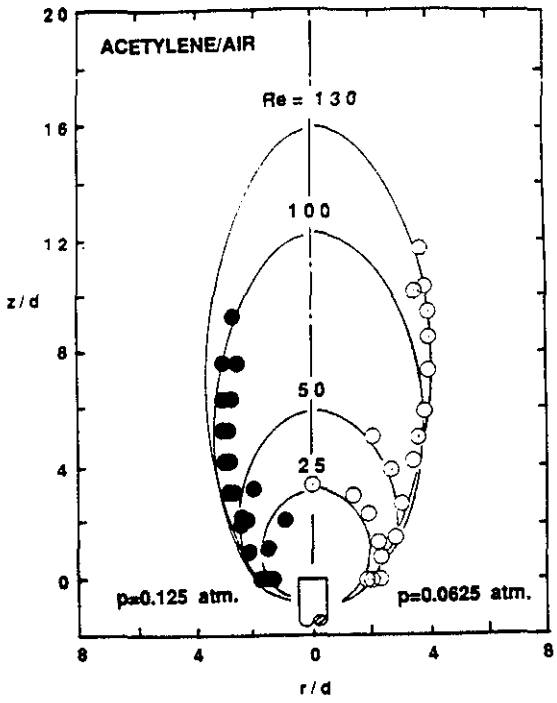


Fig. 4 Predicted and measured flame shapes for weakly-buoyant acetylene/air jet diffusion flames.

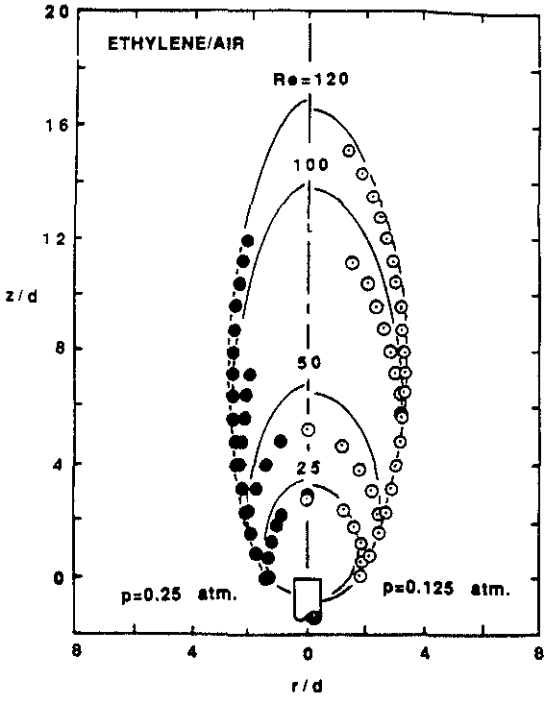


Fig. 3 Predicted and measured flame shapes for weakly-buoyant ethylene/air jet diffusion flames.

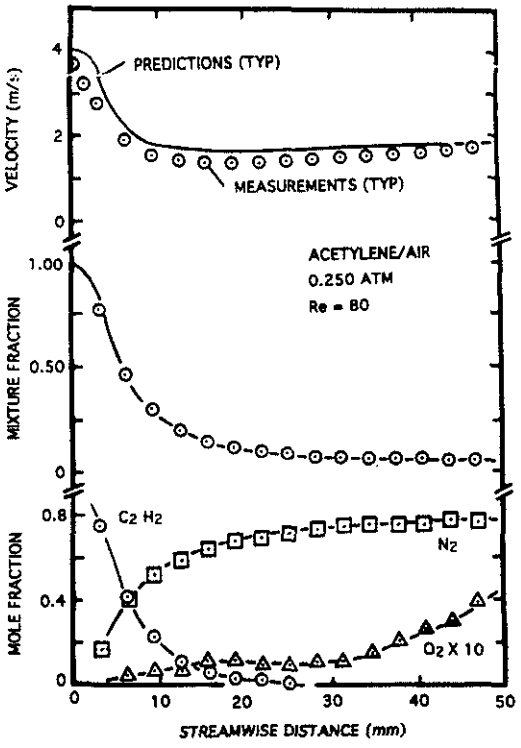


Fig. 5 Predicted and measured velocities, mixture fractions and major gas species concentrations along the axis of a weakly-buoyant acetylene/air laminar jet diffusion flame.

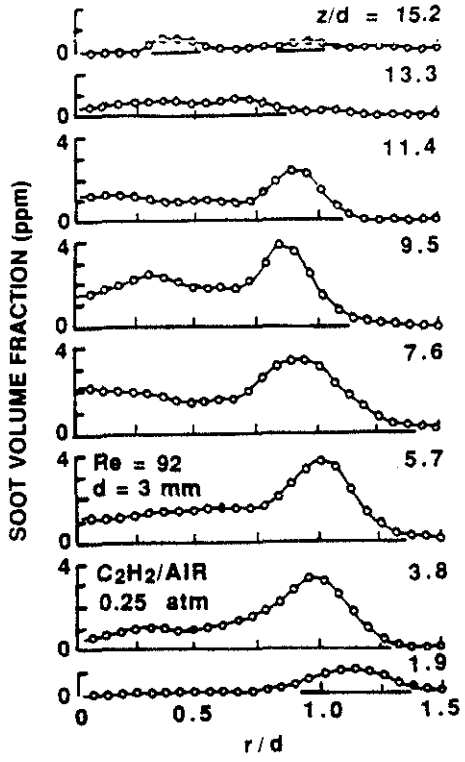


Fig. 6 Measured soot volume fraction soot distributions for the weakly-buoyant acetylene/air laminar jet diffusion flame at 0.25 atm.

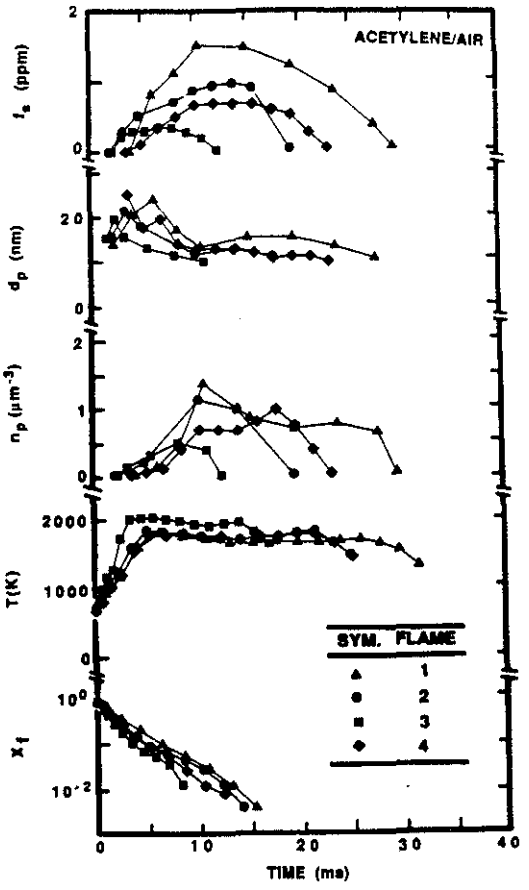


Fig. 7 Soot properties, temperatures and fuel concentrations along the axis of weakly-buoyant acetylene/air laminar jet diffusion flames.